Supplementary Information for

Interlayer breathing and shear modes in few-trilayer MoS_2 and WSe_2

Yanyuan Zhao,[1,†] Xin Luo,[2,†] Hai Li,[3] Jun Zhang,[1] Paulo Antonio Trindade Araujo,[4] Chee Kwan Gan,[2] J. Wu,[3] Hua Zhang,[3,*] Su Ying Quek,[2,*] Mildred S. Dresselhaus,[4,5] and Qihua Xiong[1,6,*]

[1]Division of Physics and Applied Physics, School of Physical and Mathematical Sciences, Nanyang Technological University, 21 Nanyang Link, Singapore 637371

[2]Institute of High Performance Computing, 1 Fusionopolis Way, #16-16 Connexis, Singapore 138632

[3]School of Materials Science and Engineering, Nanyang Technological University, 50 Nanyang Avenue, Singapore 639798

[4]Department of Electrical Engineering and Computer Science, Massachusetts Institute of Technology, Cambridge, Massachusetts 02139, United States of America

[5]Department of Physics, Massachusetts Institute of Technology, Cambridge, Massachusetts 02139, United States of America

[6]Division of Microelectronics, School of Electrical and Electronic Engineering, Nanyang Technological University, Singapore 639798

[†]These authors contribute to this work equally.

*To whom correspondence should be addressed. Email address: hzhang@ntu.edu.sg, queksy@ihpc.a-star.edu.sg and Qihua@ntu.edu.sg.

Table of Content

I. Sample Preparation and Characterizations 3

II. Vibrational Normal Modes of 1TL, 2TL and bulk MoS_2/WSe_2 4

III. Lorentzian Lineshape Analysis 5

IV. Demonstration of Breathing Mode B2 and Shear Mode S2 in Few-TL MoS_2 6

V. Substrate Effect 7

VI. First-principles Calculated Phonon Modes 7

VII. Linear Chain Model 12

References 14

I. Sample Preparation and Characterizations

Single- and few-Trilayer (TL) MoS_2 and WSe_2 samples were exfoliated from bulk single crystal MoS_2 (SPI Supplies, Inc., USA) and WSe_2 (Nanoscience Instruments, Inc., USA) and then deposited onto the freshly cleaned Si substrates with a 90 nm SiO_2 layer using the scotch tape-based mechanical exfoliation method, which is widely employed for the preparation of single- and few-layer graphene sheets.[1] The TL number of as-prepared samples is determined by both optical contrast[2] and AFM measurements.[3] Optical microscope (Eclipse LV100D, Nikon) was used to locate the single- and few-TL crystals. AFM (Dimension 3100 with Nanoscope IIIa controller, Veeco, CA, USA) was used to confirm the number of TLs by measuring the film thicknesses in tapping mode in air. Figure S-1 shows the optical and AFM images of as-prepared single- and few-TL MoS_2/WSe_2 samples, which are several microns to tens of microns in planar size. AFM images of 1-3TL MoS_2 are shown in Figure S-1a with the corresponding height profiles (Figure S-1b) taken along the colored dashed lines. The measured thickness for 1, 2 and 3TL MoS_2 is 0.8 nm, 1.4 nm and 2.1 nm, respectively; these data are consistent with the crystallography data and with previous reports[3,4] (each TL corresponds to ~ 0.7 nm). Similar to graphene, few-TL MoS_2 and WSe_2 show good optical contrast on top of 90 nm SiO_2/Si substrates, as shown in Figure S-1c and d, respectively. The optical contrast is distinctive for each thickness below 5TL and thus the number of TLs can be easily determined. For 6TL and above, the optical contrast is less distinctive and AFM measurements are necessary for the thickness determination.

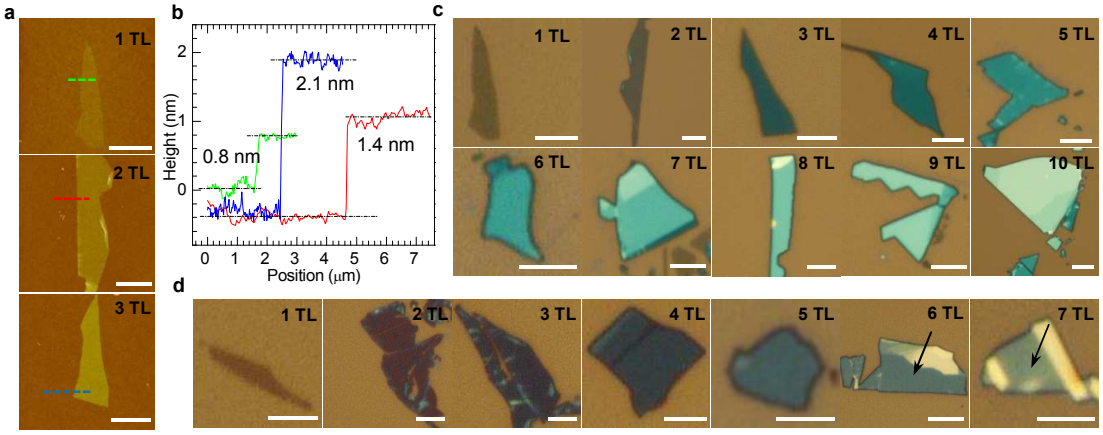

Figure S-1. Optical and AFM images of exfoliated few-TL MoS_2 and WSe_2 on 90 nm SiO_2/Si substrates. a, AFM images of 1-3TL MoS_2. **b**, height profiles taken along the green, red and blue dashed lines for 1TL, 2TL and 3TL MoS_2, respectively. **c**, optical images of 1-10TL MoS_2. Each thickness shows distinctive optical contrast. **d**, optical images of 1-7TL WSe_2. All the scale bars are 5 μm.

II. Vibrational Normal Modes of 1TL, 2TL and bulk MoS_2/WSe_2

Bulk and even-, odd-TL 2H-TX_2 all have different symmetries and therefore different irreducible representations of the phonon modes (as discussed in the main text). Group theory analysis can predict the symmetries of the vibrational phonon modes and therefore Raman/IR activities. Figure S-2 shows the normal mode displacements of the phonon modes in 1TL, 2TL and bulk MoS_2/WSe_2 crystals. The phonon mode notation and Raman/IR activity are denoted in the text underneath the vibration schematics.

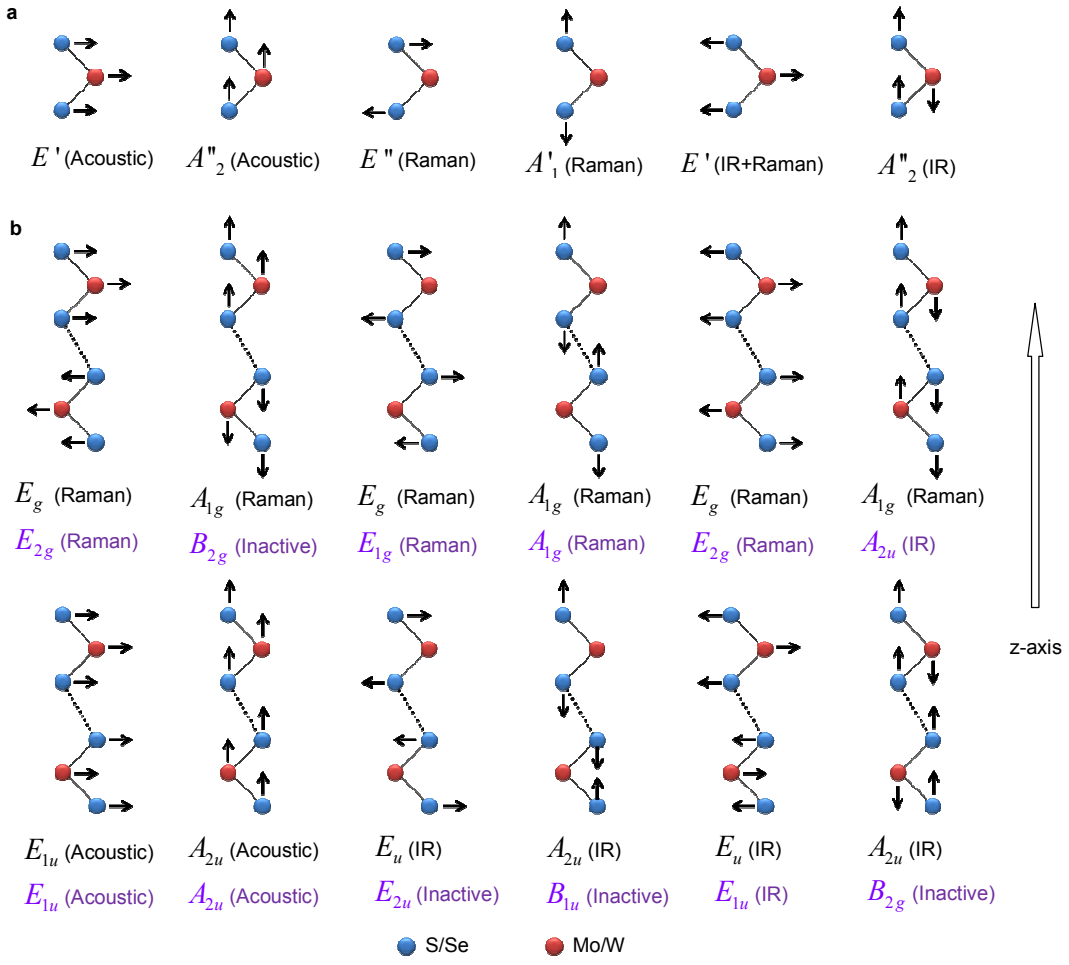

Figure S-2. Vibrational normal modes of 2H-MoS_2/WSe_2. a, normal modes of 1TL. **b**, normal modes of 2TL and bulk, both of which are the same in terms of quantity and vibrational displacements. The two normal modes in the same column form a pair of Davydov doublets. The mode notations and Raman/IR activities are labeled beneath for both 2TL (in black) and bulk (in purple).

III. Lorentzian Lineshape Analysis

All of our Raman spectra taken under the parallel polarization configuration $\bar{z}(xx)z$ exhibit a strong background in the low-frequency region, as shown in Figure S-3a, using the Stokes Raman spectrum of 4TL MoS_2 as an example. The strong low-frequency tail most likely originates from the intraband Raman scattering of free carriers in the n-doped Si substrates,[8] which are highly doped in our experiments with a resistivity of 0.001-0.002 ohm·cm. Under the perpendicular polarization configuration $\bar{z}(xy)z$, however, the low-frequency background can be largely suppressed, which is consistent with previous reports.[8,9] A careful Lorentzian lineshape analysis has been executed for all the Raman spectra presented in present work.

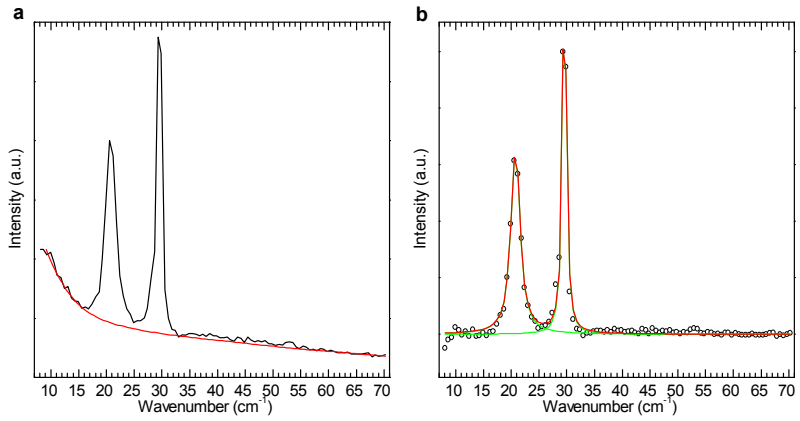

Figure S-3. Demonstration of spectrum baseline subtraction and Lorentzian analysis. a, Raman spectrum of 4TL MoS_2. The black solid line is the original data and the red line is the baseline fitted by a polynomial function. **b**, Lorentzian fitting for the baseline-subtracted spectrum (shown as black open circles). Two Lorentzian peaks (green solid line) are used and the red solid line shows the fitting result.

Firstly, we did polynomial fitting to the background, shown as the red solid line in Figure S-3a. After subtraction of the background, a Lorentzian fitting was performed to the spectrum, shown in Figure S-3b. The red solid line is the fitted result, which matches very well with the experimental data (black open circles). The green solid lines represent the Lorentzian decomposition of the fitting. The accurate Raman peak positions and full width half maximum (FWHM) intensities can be obtained from the fitting analysis. For a clear demonstration, all the Raman spectra shown in the main manuscript (Figure 1 and 2) are treated with background subtraction.

IV. Demonstration of Breathing Mode B2 and Shear Mode S2 in Few-TL MoS_2

Among all the four interlayer vibrational modes S1, S2, B1 and B2 that are experimentally observed in *N*TL MoS_2, the S2 and B2 peaks are very weak compared to the S1 and B1 peaks, and thus can barely be distinguished in Figure 2 in the manuscript, which have been normalized by the intensity of S1 to clearly display the frequency evolution trend versus thickness. To have a better demonstration of these two peaks, zoom-in Raman spectra of the original data were presented here in Figure S-4 for MoS_2 samples with thicknesses from 3 TLs to 9 TLs. Figure S-4a shows the zoom-in spectra taken under the $\bar{z}(xx)z$ polarization configuration. The B2 peaks can be clearly observed as denoted by the black asterisks from 4TL to 7TL, and scaling from 53 cm^{-1} to 35 cm^{-1}. Following the evolution trend, the B2 peak should be located at even lower frequencies in 8TL and 9TL and might be masked by the stronger S1 and S2 peaks. The S2 peak is slightly stronger than the B2 peak and shows a smaller FWHM. The red asterisks denote the S2 peaks from 6TL to 9TL. In 4TL and 5TL, the S2 peaks are submerged in the strong B1 peaks measured under the $\bar{z}(xx)z$ polarization configuration, but can be clearly distinguished under the $\bar{z}(xy)z$ polarization configuration (Figure S-4b), where the breathing modes are suppressed but the shear modes are conserved, as discussed in the previous section. The suppression of the low-frequency background under the $\bar{z}(xy)z$ polarization configuration also contributes to the evident exhibition of S2 peaks in the Raman spectra of 4-9TL (Figure S-4b). So far, the experimental observation of the interlayer shear mode S2 and the interlayer breathing mode B1 has only been unambiguously demonstrated in Few-TL MoS_2.

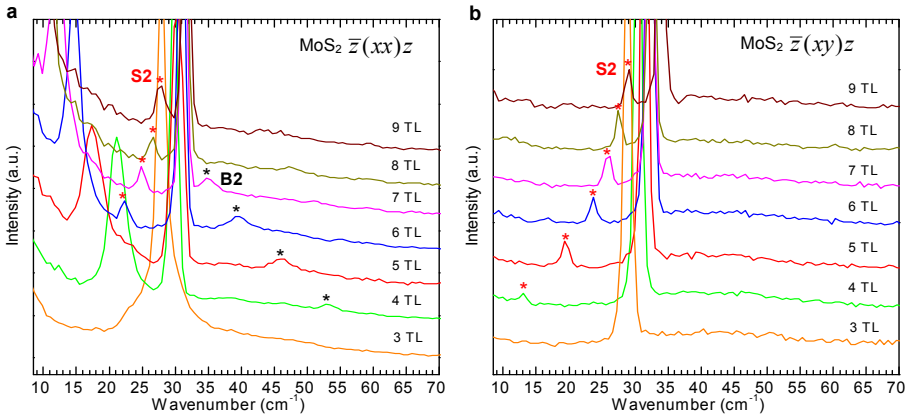

Figure S-4. Zoom-in Raman spectra for the interlayer shear mode S2 and interlayer breathing mode B2 in 3-9TL MoS_2. a, original Raman spectra measured under the $\bar{z}(xx)z$ polarization configuration. S2 modes show up as sharp peaks in 6-9TL (denoted by red asterisks), but are masked by the strong B1 peak and Rayleigh background in 5TL and 4TL, respectively. In the higher-frequency region, B2 modes are shown as weak peaks denoted by black asterisks. **b**, original Raman spectra measured under the $\bar{z}(xy)z$ polarization

configuration. S2 peaks can be observed distinctly from 4TL to 9TL (denoted by red asterisks). B2 peaks cannot be observed under this configuration.

V. Substrate Effect

All the Raman spectra discussed above were taken on 2D MoS_2/WSe_2 samples deposited on top of SiO_2/Si substrates. To investigate the substrate effect, suspended samples were also prepared for the Raman study. A thinner sample should experience a larger substrate effect than a thicker one, if there is any effect, because of its larger surface-to-volume ratio. Here, in terms of investigating the substrate effect on the interlayer vibrational phonon modes, we study 2TL MoS_2 as an example, which is the thinnest system with Raman active interlayer vibrational modes.

Figure S-5a shows the optical image of a 2TL MoS_2 sample on holed 300 nm SiO_2/Si substrates. The holed substrates are prepared by optical lithography followed by HF etching. The etched SiO_2 round holes are around 2.5 μm in diameter and 72 nm in depth. MoS_2 samples are then exfoliated on top of the holed substrates. The thickness of the sample can be determined by the optical contrast of the supported part and by AFM measurements. In Figure S-5a, the supported and suspended 2TL MoS_2 are denoted by the red and blue arrows, respectively. The Raman spectra of the corresponding areas are displayed in Figure S-5b, where both the S1 (E_{2g}^2) and B1 peaks are clearly shown. However, there is no observable difference between these two spectra in terms of both peak position and lineshape. Therefore, we conclude that the substrate effect is negligible in our Raman study.

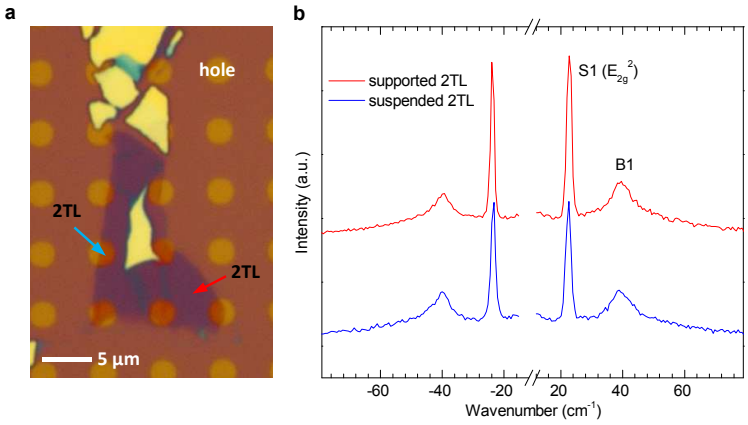

Figure S-5. Raman spectra of supported and suspended 2TL MoS_2. a, optical image of MoS_2 samples on holed 300 nm SiO_2/Si substrates. The round holes are around 2.5 μm in diameter and 72 nm in depth. The supported and suspended 2TL MoS_2 are denoted by red and blue arrows, respectively. **b**, low-frequency anti-Stokes and Stokes Raman spectra of supported and suspended 2TL MoS_2.

VI. First-principles Calculated Phonon Modes

The phonon mode notation and Raman/IR activity can be obtained from the first-principles calculations. Table S-1 summarizes the calculated number of phonon modes with

different symmetry species from 1TL to 9TL, which are consistent with the group theory predicted irreducible representations discussed in section II (SI).

Among all the 9*N* phonon modes in *N*TL system, there are *N*-1 degenerate interlayer shear modes and *N*-1 interlayerbreathing modes, as discussed above in section II. The normal mode displacements of all the interlayer shear modes and breathing modes of 2-9TL MoS_2/WSe_2 are shown in Figures S-6 and S-7, respectively. The arrow indicates the direction of displacement while its length is proportional to the displacement magnitude of that particular TL. For a given *N*TL, the normal modes are arranged from low to high frequency from left to right. The Raman/IR activity of each mode is listed below its displacement pattern. Experimentally observed S1, S2, B1 and B2 modes are color coded in blue, green, pink and orange, respectively, to be consistent with the color code in the main text.

Table S-1. The number of active phonon modes from the first-principles calculations. The Raman-active (R) and infrared-active modes (I) are identified.

Modes	R	I	I+R	R
odd (D_{3h})	A'_1	A''_2	E'	E''
1TL	1	2	2	1
3TL	4	5	5	4
5TL	7	8	8	7
7TL	10	11	11	10
9TL	13	14	14	13
Modes	R	I	I	R
even (D_{3d})	A_{1g}	A_{2u}	E_u	E_g
2TL	3	3	3	3
4TL	6	6	6	6
6TL	9	9	9	9
8TL	12	12	12	12

Figure S-6. Normal mode displacements for all the interlayer shear modes in 2-9TL MoS_2/WSe_2. The normal modes are arranged from low to high frequency, from left to right. The Raman/IR activity is listed below the displacement and the ones highlighted in blue (the highest) and green (the third highest) correspond to the S1 and S2 modes that are observed experimentally, respectively.

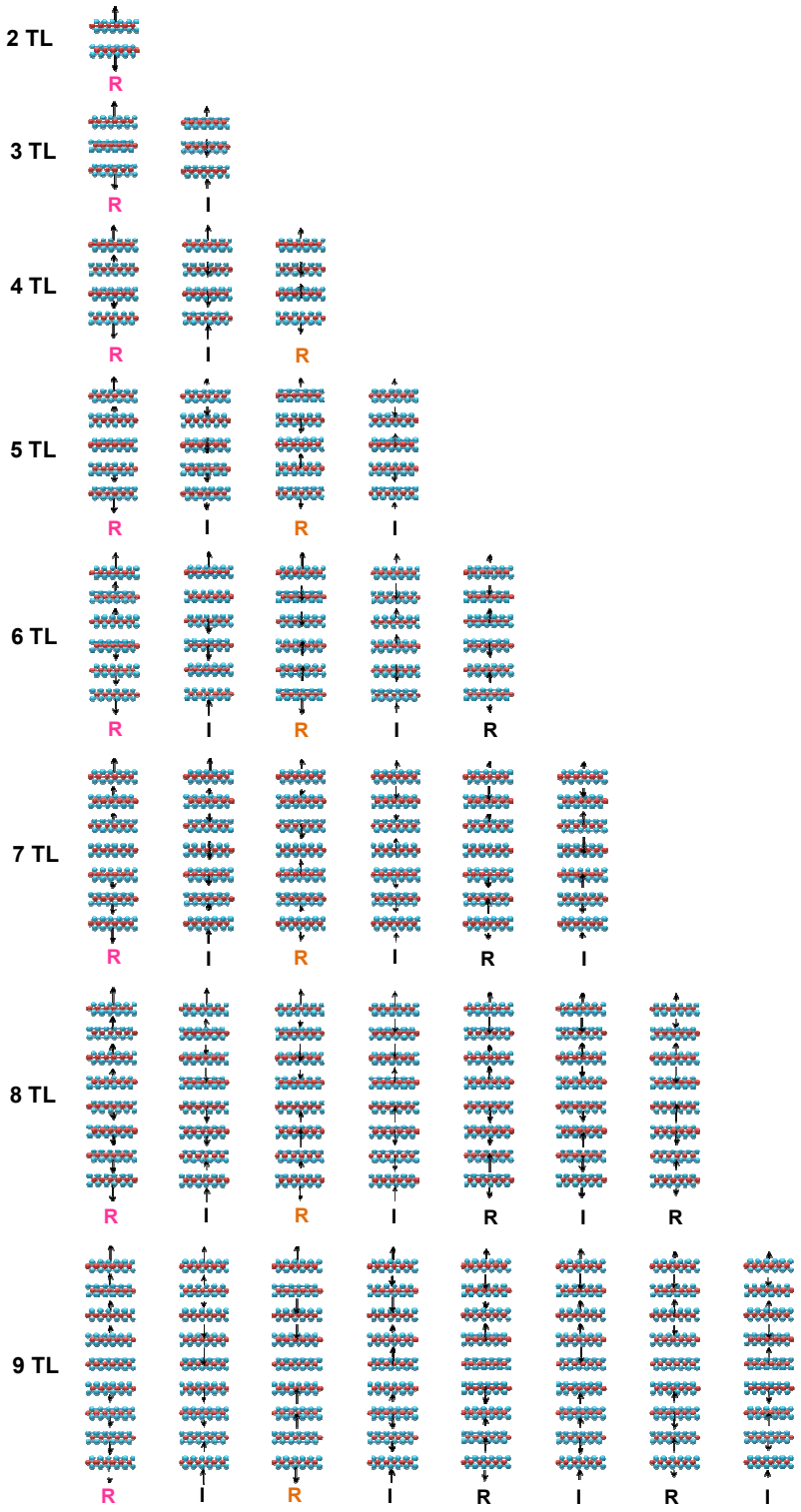

Figure S-7. Normal mode displacements for all the interlayer breathing modes in 2-9TL MoS_2/WSe_2. The normal modes are arranged from low to high frequency, from left to right. The Raman/IR activity is listed below the displacement and the ones highlighted in pink (the lowest) and orange (the third lowest) correspond to the B1 and B2 modes that are observed experimentally, respectively.

In addition to using LDA norm-conserving (LDA NC) pseudopotentials, we also compute the phonon frequencies using LDA PAW potentials, and using the vdW-DF functional[10], with Cooper's exchange interaction term.[11] Since the phonon frequencies cannot be computed with vdW-DF in QUANTUM-ESPRESSO, we adopt a force-constant approach to calculate the phonon frequencies using the vdW-DF functional.[12] In this method, we displace each atom in the primitive cell from its equilibrium position in the *x*, *y*, and *z* directions by a distance of 0.015 Å, and calculate the forces acting on each atom using the Hellmann-Feynman theorem. Subsequently, the interatomic force-constant matrix is evaluated using a central finite-difference scheme. We have used the LDA NC pseudopotential to check that the phonon frequencies as calculated with the force-constant approach are essentially the same as those obtained from the DFT method in QUANTUM-ESPRESSO. The optimized lattice constants used for the vdW-DF, LDA-NC, and LDA-PAW calculations are listed in Table S-2.

Table S-2. Optimized lattice constants of bulk, 2TL, and 3TL MoS_2 using different density functionals. *a* and *c* are, respectively, the in-plane and out-of-plane lattice parameters of bulk MoS_2.

	Lattice constants (Å)			
	vdW-DF	LDA-NC	LDA-PAW	Exp.[13]
Bulk (*a*)	3.1914	3.169	3.1306	3.1602
Bulk (*c*)	12.258	12.086	12.062	12.294
2TL (*a*)	3.1904	3.1677	3.13	3.1602
3TL (*a*)	3.1905	3.1682	3.1304	3.1602

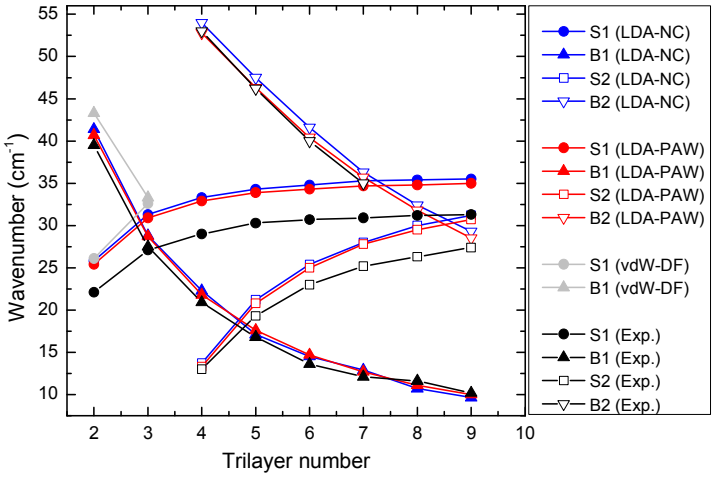

Figure S-8. The frequency evolutions of the interlayer shear and breathing modes in few-TL MoS_2. Both the LDA norm-conserving pseudopotentials (LDA-NC) and the projector-augmented wave potentials (LDA-PAW) were used for 2-9TL. The van der Waals density functional (vdW-DF) with Cooper's exchange[11] is applied to the 2TL and 3TL systems.

Figure S-8 shows the comparison of the frequency evolutions using both the LDA-PAW and LDA-NC method, where the results are essentially the same. The PAW method is considered as being accurate for use as an all-electron method. Thus, the consistency between the LDA-PAW and LDA-NC methods indicated that the norm-conserving pseudopotentials used here can give an accurate description of the frequencies. On the other hand, the vdW-DF result for the 2TL and 3TL systems in Figure S-8 shows that it overestimates the low frequency modes. Compared with the experimental data, the discrepancy of the breathing modes (B1 and B2) is smaller than that of the shear modes.

VII. Linear Chain Model

As discussed in the main text, the displacement of j-th TL eigenvector for α-th breathing ($\beta=z$) or shearing mode ($\beta=x, y$) can be fitted well by the eigenmodes

$$u_{j,\beta}^{\alpha} \propto \cos\left[\frac{(\alpha-1)(2j-1)\pi}{2N}\right] \tag{S9}$$

and corresponding phonon frequencies (in cm^{-1})

$$\omega_{\alpha} = \sqrt{\frac{K}{2\mu\pi^2 c^2}\left(1-\cos\left(\frac{(\alpha-1)\pi}{N}\right)\right)} \tag{S10}$$

where K is the force constant, N is the total number of TLs, j labels the specific TL in NTL. α goes from 1 to N, and μ is the TL mass per unit area and c is the speed of light.

The LDA calculated phonon frequencies can be fitted by a linear chain model. As shown in Figure S-9, by fitting all shear modes frequencies for each NTL system in MoS_2, we found that the interlayer shear force constants K_x remain unchanged for different thickness thin films (NTL, N changes from 2 to 9). The same holds for the fitting of all breathing modes in MoS_2, as shown in Figure S-10. The breathing force constant K_z derived from the fitting is three times larger than the shear force constant K_x, indicating strong elastic anisotropic behavior in these layer compound materials.

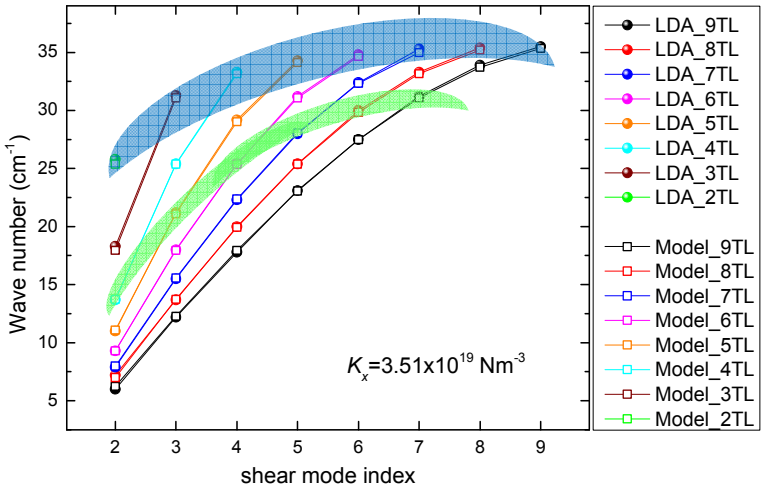

Figure S-9. With only one K_x, all the shear modes from 2TL to 9TL MoS_2 can be fitted well by the linear chain model described in the main text. The modes shadowed in blue and green correspond to experimentally observed S1 and S2 modes, respectively.

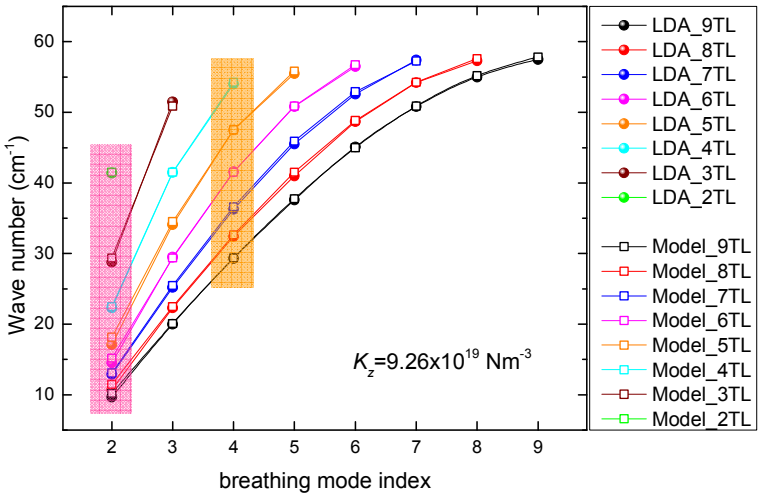

Figure S-10. With only one K_z, all the breathing modes from 2TL to 9TL MoS_2 can be fitted well by a linear chain model. The modes shadowed in pink and orange correspond to experimentally observed B1 and B2 modes, respectively.

References

1 K. S. Novoselov, D. Jiang, F. Schedin et al., *P. Natl. Acad. Sci. USA.* **102** (30), 10451 (2005).

2 Hai Li, Gang Lu, Zongyou Yin et al., *Small* **8** (5), 682 (2012).

3 Hai Li, Zongyou Yin, Qiyuan He et al., *Small* **8** (1), 63 (2012).

4 M. M. Benameur, B. Radisavljevic, J. S. Heron et al., *Nanotechnology* **22** (12) (2011); B. Radisavljevic, A. Radenovic, J. Brivio et al., *Nat. Nanotechnol.* **6** (3), 147 (2011).

5 J. L. Verble and T. J. Wieting, *Phys. Rev. Lett.* **25** (6), 362 (1970).

6 T. J. Wieting and J. L. Verble, *Phys. Rev. B* **3** (12), 4286 (1971).

7 T. C. Damen, S. P. S. Porto, and B. Tell, *Phys. Rev.* **142** (2), 570 (1966).

8 Meera Chandrasekhar, Manuel Cardona, and Evan O. Kane, *Phys. Rev. B* **16** (8), 3579 (1977).

9 P. H. Tan, W. P. Han, W. J. Zhao et al., *Nat. Mater.* **11** (4), 294 (2012).

10 Guillermo Román-Pérez and José M. Soler, *Phys. Rev. Lett.* **103** (9), 096102 (2009); M. Dion, H. Rydberg, E. Schröder et al., *Phys. Rev. Lett.* **92** (24), 246401 (2004).

11 Valentino R. Cooper, *Phys. Rev. B* **81** (16), 161104 (2010).

12 G. Kresse, J. Furthmüller, and J. Hafner, *EPL (Europhysics Letters)* **32** (9), 729 (1995); C. K. Gan, Y. P. Feng, and D. J. Srolovitz, *Phys. Rev. B* **73** (23), 235214 (2006).

13 K. K. Kam and B. A. Parkinson, *The Journal of Physical Chemistry* **86** (4), 463 (1982).

14 Alberto Carpinteri, *Structural Mechanics: A Unified Approach* (Taylor & Francis, 1997).

15 S Q Wang and H Q Ye, *J. Phys.: Condens. Matter* **15** (30), 5307 (2003).